ASSESSMENT OF ADVANCED TECHNOLOGIES FOR HIGH PERFORMANCE SINGLE-ENGINE BUSINESS AIRPLANES

David L. Kohlman* and Bruce J. Holmes**

Paper No. ICAS-82-1.4.3
13th Congress of the International Council of the
Aeronautical Sciences and the
AIAA Aircraft Systems and Technology Meeting
August 22-27, 1982

SYMBOLS

AR	aspect ratio
BHP	brake horsepower
C_d	section drag coefficient
C_L	lift coefficient
C_l	section lift coefficient
h	altitude
L/D	lift-to-drag ratio
$(L/D)_m$	maximum lift-to-drag ratio
R	range
R_c	Reynolds number based on chord length
S	wing area
V	true airspeed
V_m	true airspeed for maximum L/D
V_{S_o}	equivalent stall airspeed at maximum gross weight in landing configuration
W	weight
W_p	payload

Subscripts

max	maximum
cr	cruise
TO	takeoff

* President, Kohlman Aviation Corporation, Lawrence, Kansas.

** Aerospace Technologist, NASA Langley Research Center, Hampton, Virginia.

Acronyms

GASP	General Aviation Synthesis Program
SIR	Spark Ignited Reciprocating Engine
FAR	Federal Aviation Regulations
FAA	Federal Aviation Administration
NASA	National Aeronautics & Space Administration

INTRODUCTION

THE IMPRESSIVE GROWTH in recent years in the use of general aviation aircraft for transportation of people and cargo has occurred largely because of the value we place on time. More directly, pressures created by airline deregulation, decentralization of businesses, and reduced highway speed limits have led to increased use of today's general aviation aircraft. Presently, the U.S. general aviation fleet of 208,000 aircraft flies 42-million hours annually. According to Federal Aviation Administration forecasts[1], during the next decade, the fleet may grow to between 268,000 and 346,000 aircraft flying between 55-million and 71-million hours annually. By one measure, to the extent that aircraft can be used to increase industrial productivity and in turn standard of living, more growth is better. In the future, the growth in the role of general aviation in our national transportation system will depend largely on the successful development of advanced, more fuel efficient, and even better performing airplanes. This paper illustrates the potential for significant improvements in the mission performance of the high-performance single-engine airplane through the application of advanced aerodynamic,

propulsion, and structural technologies. The data presented illustrate the benefits of individual and integrated technologies on wing design parameters, cruise power requirements, and fuel efficiency for a specified mission. In addition, sensitivity of the design parameters to variations in mission speed, range and payload were analyzed.

The baseline mission selected for analysis (see Table 1 and Figure 1) is cruise speed V_{cr} = 300 knots, cruise range R_{cr} = 1300 n.mi. (no reserves), cruise altitude h_{cr} = 10,700 m (35,000 ft), and payload W_p = 5338 N (1200 lb or six passengers including crew with baggage). These performance objectives are significant in that they represent approximately a 100-percent increase in cruise speed and range (at maximum cruise speed) over current single-engine business airplanes. This single-engine mission performance is comparable to that for current high-performance twin-engine, turbo-prop airplanes. Previous studies[2-4] have illustrated the potential for achieving these high levels of performance and fuel efficiency with current aerodynamic, structural and propulsion technologies considered individually. The present analysis considers the potential benefits of advanced technologies applied to the design problem individually and integrally. Specifically, the benefits of the technologies categorized in Table 2 are analyzed.

Typically, in general aviation airplane design, cruise speed, V_{cr}, is much greater than the speed where maximum lift-to-drag ratio occurs V_m; hence, cruise lift-to-drag ratio $(L/D)_{cr}$, is much less than the maximum lift-to-drag ratio, $(L/D)_m$, for current airplanes. This fact results from constraints placed on wing loading by current design practices and by Federal Aviation Regulations (FAR's). In current practice, wing loading

Table 1 Baseline Mission

Payload	1200 lb (including 200 lb crew)
Range	1300 nm (no reserves)
Cruise speed	298 knots
Cruise altitude	35,000 ft
Takeoff distance over a 50 ft obstacle	< 3000 ft

Table 2 Design Technologies Assessed

PROPULSION

- GATE (ref. 6)
- Rotary
- Diesel
- Advanced spark-ignited reciprocating (SIR)

NATURAL LAMINAR FLOW

- Wing
- Fuselage

HIGH LIFT

- Leading edge devices
- Trailing edge devices

CONFIGURATIONS

- Baseline
- Pusher propeller
- Canard

MATERIALS

- Aluminum
- Composites

is constrained by present high-lift system design practice coupled with FAR Paragraph 23.49 which states that "V_{s_o} at maximum weight may not exceed 61 knots for . . . single-engine airplanes . . ." For this study, wing loading is assumed to be unconstrained by these currently limitations in order to analyze what design benefits accrue to higher values of wing loading. These higher wing loadings permit V_m to increase in a fashion which produces a closer match between V_m and cruise speed. Then $(L/D)_{cr}$ occurs closer to $(L/D)_m$ and cruise fuel efficiency should improve. The design approach for this study involves varying wing geometry on a fixed fuselage design. The term "cruise matched" is used herein to denote the relationship between design wing loading, power loading, and the ratios $(L/D)_{cr}/(L/D)_m$ and V_{cr}/V_m.

It has been illustrated in past studies[2,3,5] that wing loadings higher than presently practiced (due to existing stall-speed regulations) offer significant benefits in the design of this class of airplanes.

Clearly the proposed use of high values of design wing loadings for a single-engine airplane needs further discussion, especially regarding safety. Essentially, the discussion tends towards debate of risks and benefits. The risks of high wing loading are associated with high approach and landing speeds; the benefits are associated with fuel efficiency, airplane performance, and ride smoothness in turbulence. This is a very large debate and the present study claims only to present the benefits of cruise-matched design wing loadings. However, it may be instructional to look briefly at the origins of the present single-engine stall-speed regulation. The history behind the current regulations dates back to the U.S. Department of Commerce Aeronautics Branch, Aeronautics Bulletin No. 7-A, January 1, 1932. It is stated therein that

all airplanes must "land at a speed not exceeding 65 miles per hour, except that airplanes which are neither designed nor used to carry passengers shall land at a speed not exceeding 70 miles per hour," (Section 76, Paragraph (A) (1)). Undoubtedly, this requirement was based on operational constraints (field lengths and surfaces, for example) as well as crash survivability. However, it might be argued that technology has radically changed operational and crashworthiness aspects of aircraft design in the nearly five decades since 1932.

In light of the potential benefits presented here, special consideration of stall-speed requirements for a high-performance, single-engine class of airplanes may be warranted.

Data reported in this paper were obtained by using the General Aviation Synthesis Program (GASP)[6] to provide more detailed, accurate mission performance calculations than have been previously obtained. A very attractive feature of GASP is its ability to rapidly size an airplane-engine combination, with specified configuration constraints, to exactly meet given mission requirements. Note that the effects of various geometry changes, propulsion systems, and application of technologies are presented in terms of completely resized, mission-matched configurations in each case.

BASELINE AIRPLANE ANALYSIS

A baseline configuration was chosen to represent current technology performance capability, although no current production airplane has a similar mission or performance capability. It serves as a benchmark to which other configurations employing a variety of technologies can be compared.

The baseline configuration was defined primarily by the baseline mission (Table 1) and the choice of engine, wing loading, and aspect ratio.

The Pratt and Whitney PT6A-45A turboprop engine, a currently available model, was chosen as the baseline engine. During parametric studies that sized the airplane to the baseline mission, a rubber engine (same specifics as published for the production engine while varying weight and power) was assumed. A 10 horsepower penalty for pressurization and cabin cooling at 35,000 ft was applied.

Based on previous studies, the baseline configuration was assigned a wing loading of 40 lb/ft^2 and an aspect ratio of 8. The computer program, GASP, was then used to size the airplane to meet the baseline mission requirements. The results are presented in Table 3.

Other assumptions made in computing the characteristics of the baseline configuration are:

- tractor propeller configuration
- turbulent boundary layer on wings and fuselage
- conventional aluminum structure
- single-slotted Fowler flaps, 75% span
- pressurized cabin, 8 psf differential pressure

Effect of Aspect Ratio

Figure 2 shows the effect of aspect ratio on gross weight, average cruise specific range, and total mission fuel for various wing loadings. In terms of total fuel used and specific range, performance improves as aspect ratio increases even beyond 12, except for the low wing loading of 30 psf. However, it appears that 12 is close to the practical upper

Table 3 Description and Performance of the Baseline HIPS Airplane

Configuration Data:	
gross weight	4794 lb
wing area	119.9 ft^2
wing loading	40 psf
aspect ratio	8
wing fuel volume	186.7 gal
empty weight	2669 lb
maximum payload	1200 lb
engine	P&W PT6A-45A
sea level max. power	1289 hp
propulsion system weight	801 lb
Performance:	
cruise speed	298 kt
cruise altitude	35,000 ft
range (max. payload)	1300 nm
average cruise specific range	1.63 nm/lb
total fuel for max. payload mission	991 lb
range (max. fuel)	1825 nm
takeoff distance to 50 ft	1879 ft
landing distance from 50 ft	1215 ft
stall speed (takeoff, max. gross weight)	75.9 kt
stall speed (landing, max. gross weight)	64.9 kt
stall speed (landing, end of mission)	58.0 kt
$(L/D)_{max}$	14.87
$(L/D)_{cruise}$ (average)	12.96

limit because wing fuel volume becomes insufficient at the combination of AR = 12 and wing loading of 50 psf; very small tip tanks are required at that point. In addition, improvements in fuel economy and gross weight appear to diminish rapidly as aspect ratio increases beyond 12. Not only does fuel volume become a problem at these high aspect ratios, but space for control system and landing gear components and flap mechanisms also becomes quite limited.

At the higher wing loadings, increasing the aspect ratio from 8 to 12 results in fuel savings ranging between 6 and 8.5 percent.

Effect of Wing Loading

Figure 3 shows the effect of wing loading on gross weight, average cruise specific range, and total mission fuel for various aspect ratios. The most obvious result is that fuel economy and gross weight are optimized at wing loadings between 45 and 50 psf. High aspect ratios favor slightly higher wing loading.

Of course, as wing loading increases, stall speed increases also. There are certain constraints. As discussed earlier, single engine airplanes are limited by FAR Part 23 to a maximum stall speed of 61 knots in the landing configuration. This boundary is shown in Figure 3. The maximum lift coefficient used to compute this boundary is predicted by GASP to be in the range of 2.8 to 2.9. This is probably somewhat optimistic, even for well designed Fowler flaps, but the possible error in predicted stall speed is not drastic. For the sake of comparison, note that the experimental single-engine Redhawk airplane (Reference 7) with 50% span Fowler flaps and full-span Kruger flaps demonstrated a trimmed $C_{L_{max}}$ of 2.73. The twin-engine ATLIT experimental airplane (Reference 8)

with full-span Fowler flaps and no leading edge devices produced a trimmed $C_{L_{max}}$ of 3.03.

Using GASP predictions, stall speed at the optimum wing loading is very close to 70 knots. The 9 knot increase above the FAR 23 constraint allows approximately a 3 percent decrease in gross weight and almost 6 percent increase in fuel efficiency. For a simpler flap system or more conservative $C_{L_{max}}$ predictions, the improvements possible by relaxing the 61 knot rule are much more substantial. When one realizes that most current single engine airplanes have a wing loading between 17 and 25 psf, it becomes evident that quite substantial gains in fuel economy are still possible with increases in wing loading and cruise altitude.

The primary result of cruising at high altitude and high wing loading is that the cruise L/D is relatively close to maximum L/D at a reasonably high cruise speed. This is illustrated in Figure 4. As wing loading is increased, cruise L/D approaches closer to maximum L/D. However, for a given cruise speed, specific range maximizes before L/D at cruise reaches maximum L/D. The reason is that as wing loading increases, maximum L/D decreases because the size of the fuselage relative to the wing increases. So even though one might cruise at $(L/D)_{max}$ with a sufficiently high wing loading, a higher cruise L/D can be achieved with a somewhat lower wing loading.

Of course, one can always decrease the cruise speed of a given configuration until flight at maximum specific range is achieved. If this is done for the baseline configuration, cruise speed is decreased from 298 to 272 knots and average specific range becomes 1.75 nm/lb, a 7.6 percent increase. Range increases to 1410 nm. For this case, GASP

maximizes specific range at start of cruise, rather than cruise L/D. This mission is not flown at $(L/D)_{max}$ because PT6-A45 engine fuel consumption and propeller efficiency are functions of airspeed. Of course, specific range is the preferred parameter to maximize.

The effect of wing loading on approach speed, stall speed, and FAR field length required for landing is shown in Figure 5. It is clear that the landing field length required is well under the design target of 3000 ft for all wing loadings investigated*. FAR field length is computed by dividing the actual landing distance over a 50 ft obstacle by the factor 0.6. Stall speeds are shown for both maximum gross weight and the weight at the end of the baseline mission.

TECHNOLOGY BENEFITS

Natural Laminar Flow

Recent NASA flight experiments[9,10,11] investigating natural laminar flow phenomena have proven that modern metal or composite general aviation production wing surfaces can be sufficiently free of waviness and roughness to support extensive runs of natural laminar flow. These recent experiments include measurements on the all-composite Bellanca Skyrocket II airplane illustrated in Figure 6[10]. Section drag was determined by wake probe measurements to be $C_d = 0.0047$ at $C_\ell = 0.2$, $R_c = 9.7 \times 10^6$. At $C_\ell = 0.3$, transition was observed to be at the 46 percent chord position on both the upper and lower surfaces. These observations match theoretical predictions well[10] for the NACA 63_2-215 airfoil incorporated on the Skyrocket wing.

Based on these experiences, the present analysis incorporated an

---

*Throughout this paper, wing loading is specified for maximum gross weight unless otherwise stated.

NLF(1)-0416 airfoil, a modern natural laminar flow section[9], for the laminar flow trade studies. This airfoil at cruise achieves 40 percent chord upper surface and 50 percent chord lower surface laminar flow at $R_c = 4.0 \times 10^6$. The airfoil was designed for a high section maximum lift capability and achieves $C_{\ell_{max}} = 1.69$ at $R_c = 3.0 \times 10^6$. The benefits of laminar flow on portions of the fuselage and empennage were studied as well. On the fuselage, 21 percent of body length was assumed laminar (back to the windshield). No credit was taken for laminar flow on the empennage.

The existence of laminar flow on the fuselage is enhanced by having an aft-mounted pusher propeller to eliminate the unsteady flow field at the nose. This configuration also eliminates the scrubbing drag penalty due to the fuselage being immersed in the propwash.

The effects of a pusher propeller, laminar fuselage flow, and a natural laminar flow wing were analyzed separately. Results are presented in Table 4. The elimination of scrubbing drag on the fuselage results in a 3.4 percent fuel saving. Adding the benefit of laminar flow on the fuselage results in a total fuel saving of 6.8 percent and a 114 lb decrease in gross weight. The laminar flow wing produces a 14 percent fuel saving and a 284 lb reduction in gross weight.

In practice, the principle challenge to the practical use of natural laminar flow on this class of airplanes is protection of the aerodynamic surfaces from ice and insect contamination. Developments in porous leading edge ice protection systems[13] offer promise for insect contamination protection as well. Wind tunnel[14] and flight[15] experiments have shown that insect contamination is prevented by keeping the airfoil leading edge region wet. Future wind tunnel, icing tunnel, and flight

Table 4 Comparison of Baseline Airplane and Baseline with Pusher Propeller, Pusher Propeller and Laminar Flow on Forward Fuselage, and Baseline with NLF(1)-0416 Airfoil

Configuration Data:	Baseline	Pusher Propeller, no fuselage laminar flow	Pusher Propeller and laminar flow on fuselage	Baseline with NLF(1)-0416 Laminar Wing
gross weight	4794 lb	4727	4680 lb	4510
wing area	119.9 ft^2	118.2	117.0 ft^2	112.8 ft^2
wing loading	40.0 psf	40.0 psf	40.0 psf	40.0 psf
aspect ratio	8	8	8	8
empty weight	2649 lb	2614 lb	2588 lb	2499 lb
sea level max. power	1275 hp	1235 hp	1206 hp	1103 hp
Performance:				
average cruise specific range	1.63 nm/lb	1.69 nm/lb	1.73 nm/lb	1.90 nm/lb
total fuel for max. payload mission (1300 nm range)	946 lb	914 lb	891 lb	812 lb
range (max. fuel)	1823 nm	1853 nm	1874 nm	1952 nm
$(L/D)_{max}$	14.87	15.09	15.26	16.34
$(L/D)_{cruise\ (average)}$	12.96	13.26	13.47	14.29

experiments by NASA are planned with a porous leading edge configuration illustrated in Figure 7. Candidate porous materials for the leading edges include electron or laser beam drilled sheet titanium and porous composite materials. The purpose of these experiments is to validate this ice and insect protection system concept for use on natural laminar flow airfoils.

Propulsion Systems

A considerable amount of research and development effort has been devoted to the field of general aviation propulsion in recent years. The programs have focused on three different approaches: the development of a low-cost turbine engine for general aviation (the GATE program), the evolutionary improvement of the piston engine through advanced materials and design innovations, and developing advanced rotary and diesel engines for use in airplanes.

In this chapter the performance of a high performance single-engine airplane is analyzed using four different advanced technology engines:

1. the low-cost General Aviation Turbine Engine (GATE)
2. a spark-ignited reciprocating engine (SIR)
3. a diesel engine
4. a rotary engine.

It is not possible to fully discuss the design characteristics and details of these engines in this paper. A summary of the primary characteristics used for this study is presented in Tables 5 through 8. Further details are available in References 16-19.

Weight and fuel consumption for each engine reflects a 10 horsepower requirement at cruise for pressurization and cabin cooling.

Table 5 GATE Engine Summary

Design Features

- Low-cost GATE technology (40% cost reduction)
- 12:1 pressure ratio
- Turbine inlet temperature: 2140°F (cruise)
- Low-cost digital electronic fuel control
- Laminated, radial flow high pressure turbine

Weight

$$\text{Weight: } W = \left[\left(\frac{BHP_{TO} + 29.4}{494} \right)^{.72} + 1 \right] (176)$$

where: W = weight of engine + accessories, lb

BHP_{TO} = takeoff brake horsepower

Lapse Rate and Fuel Consumption

Functions of V and altitude.
See Reference 16.

Table 6 Very Advanced Spark Ignited Engine Summary

Design Features

- Stratified charge
- Multifuel capability
- Very advanced turbocharging
- Turbocompounded
- Substantial use of titanium
- Horizontally opposed
- Air cooled

Weight and Power

Weight: $W = \left[\left(\frac{BHP_{TO} + 15.4}{350} \right)^{.816} (405) + 121 \right]$ (lb)

Power:

Altitude (feet)	Power available as fraction of sea level maximum	
	Maximum Continuous	Continuous Cruise
0	1.0	0.651
5K	1.04	0.694
15K	1.029	0.734
25K	0.903	0.714
35K	0.70	0.651

Fuel Consumption

Altitude (feet)	Specific Fuel Consumption lb/bhp/hr	
	Maximum Continuous	Cruise
0 to 35K	.334	.331

Table 7 Very Advanced Diesel Engine Summary

Design Features

- Radial, air cooled
- Two-stroke cycle
- Highly turbocharged
- Catalytic combustor in turbocharger loop for starting and high altitude operation
- Synthetic oil (high engine temperature)
- 65% cooling drag reduction
- Ceramic piston top and cylinder walls

Weight and Power

Weight: $W = 11.879[BHP_{TO} + 30]^{.581} + 121$ (lb)

Power:

Altitude (feet)	Power available as fraction of sea level maximum: Maximum Continuous Cruise	Economy Cruise
0 to 17K	1.0	0.83
20K	0.889	0.708
25K	0.694	0.572
30K	0.514	0.425
35K	0.333	0.275

Fuel Consumption

Altitude (feet)	Specific fuel Consumption lb/hp/hr: Maximum Continuous	Economy Cruise
0 to 17K	0.313	0.290
20K	0.317	0.293
25K	0.323	0.293
30K	0.330	0.305
35K	0.336	0.311

Table 8 Very Advanced Rotary Engine Summary

Design Features

- Stratified charge using dual injectors
- Multifuel capability
- Very advanced turbocharging
- Liquid cooled--zero cooling drag
- Retracting apex seals
- Zirconium oxide insulated rotor face

Weight and Power

Weight: $W = .53BHP_{TO} + 233$ (lb)

Power:

Altitude (feet)	Power available as fraction of sea level maximum	
	Maximum Continuous	Continuous Cruise
0 to 21K	1.0	0.781
25K	0.859	0.781
30K	0.709	0.65
35K	0.594	0.55

Fuel Consumption

Altitude (feet)	Specific Fuel Consumption lb/bhp/hr	
	Maximum Continuous	Cruise
0 to 25K	0.372	0.355
30K	0.370	0.354
35K	0.378	0.357

Parametric trade studies were carried out using different values of wing loading and aspect ratio for each propulsion system. All configurations were assumed to employ a pusher propeller, laminar flow wing, and have some laminar flow on the fuselage. A conventional wing and tail planform was used along with an aluminum primary structure. All configurations were sized to meet the baseline mission performance specification.

Figures 8-11 show the takeoff gross weight, cruise specific range, and total fuel used for the baseline mission as a function of wing loading, for aspect ratios of 10 and 12, for each propulsion system. Several significant results are apparent. For the cruise speed and altitude chosen, the optimum wing loading in terms of fuel consumption is between 45 and 50 psf, regardless of engine type. It appears that aspect ratios higher than 12 would result in even better fuel performance than shown, but it is believed that 12 represents a practical upper limit because of internal fuel volume, structural elasticity, and internal space for control system and landing gear components. Note also that the curves are very flat at these optimum wing loadings, thus one would tend to choose a wing loading that is on the low side of the optimum value so that takeoff and landing speeds are as low as possible, consistent with efficient cruise performance.

Another observation is of interest regarding gross weight. In every case but one, the takeoff gross weight is lowered with an increase in aspect ratio from 10 to 12, even though wing weight will increase as aspect ratio goes up. However, this structural weight increase is more than offset by the decrease in fuel weight and engine weight resulting from the improvement in aerodynamic efficiency. The exception is the GATE configuration, for which the higher aspect ratio produces a very slightly higher

gross weight. This results from the fact that the GATE engine is very light weight, thus a reduction in engine weight due to lower drag is not sufficient to overcome the increase in wing weight.

Table 9 presents a comparison of the airplanes, sized for the 1300 nm baseline mission, with four different advanced technology engines. Near optimum values of wing loading and an aspect ratio of 12 are used for the comparison.

The heaviest airplane is diesel powered; the lightest is the GATE, a result that corresponds directly with engine weight. On the other hand, the most fuel efficient airplane is rotary powered, a result of low engine weight, excellent specific fuel consumption, and negligible cooling drag. The GATE engine, with the highest sfc of all, uses the most fuel of any of the four configurations.

The diesel engine has the best specific fuel consumption, but this is offset by the relatively high specific weight and the high lapse rate of the diesel, which results in a sea level power rating about twice as large as the rotary and SIR.

As might be expected, the maximum and cruise L/D values are very nearly the same for all four configurations.

Considering fuel efficiency, gross weight, engine size, engine cooling, and multifuel capability, the rotary powered airplane appears to be the most attractive configuration in this study. It is of interest at this point to note that the rotary powered configuration in Table 9 represents a 54% reduction in fuel used and a 15% reduction in gross weight compared to the original baseline configuration, with no change in mission performance.

Table 9 Comparison of Single-Engine Airplane With Four Different Advanced Technology Engines

	GATE	SIR	DIESEL	ROTARY
CONFIGURATION DATA				
gross weight, lb	4045	4340	4458	4062
wing area, ft^2	89.9	86.8	89.2	81.2
wing loading, lb/ft^2	45.0	50.0	50.0	50.0
aspect ratio	12	12	12	12
empty weight, lb	2285	2673	2798	2406
sea level max. power, hp	806	573	1170	615
PERFORMANCE				
average cruise specific range, nm/lb	2.73	3.08	3.21	3.20
total fuel for max. payload mission, lb (1300 nm range)	560	468	461	456
range (max. fuel), nm	1916	1864	1714	1564
(L/D) max	18.77	18.04	18.2	18.16
(L/D) cruise (average)	15.92	16.03	16.2	16.13

NOTE: All configurations incorporate pusher propeller, laminar flow wing, partial laminar flow fuselage.

High Lift Systems

Possible performance improvements were computed for three types of high lift devices: leading-edge flaps, single-slotted Fowler flaps, and double-slotted Fowler flaps.

The increments in maximum lift coefficient computed by GASP were considered to be too high in all cases, thus stall speeds were computed using $C_{L_{max}}$ values based on data from References 22 and 23.

The penalties for meeting the 61 kt single-engine stall speed requirement of the FAR's were found by comparing fuel used, total weight, and engine size for an airplane with the wing loading necessary for a 61 kt stall speed with values for an airplane with an optimum wing loading based on cruise specific range. This optimum wing loading is very close to 50 lb/ft^2.

Table 10 shows the results of the study. Clearly, the full span flaps result in only a small penalty if the 61 knot stall requirement must be met, but the cost of the flap system and the necessary spoiler roll control system will not be negligible. GASP predictions indicate only a 10 lb maximum weight difference between the various flap systems, thus the gross weight and fuel used at optimum wing loading will differ little between the configurations in Table 10. Takeoff and landing distances for all the flap systems and wing loadings studied are well under the 3000 ft limit.

Although leading edge devices might allow an increase of 0.3 to 0.5 in $C_{L_{max}}$, thus increasing the wing loading limit for a 61 kt stall speed to 46-48.5 psf for full-span, double-slotted flaps and 40.7-43.2 psf for

Table 10 Stall Speeds and Wing Loading Limits for Various Fowler Flap Configurations

Airfoil and Flap Type		PT6 Engine, Baseline, NACA 65_2-415 Airfoil, Single-Slotted 0.75 Span Flap $C_{L_{max}}$ = 2.6	Rotary Engine, NLF-0416 Airfoil, Single-Slotted 0.75 Span Flap $C_{L_{max}}$ = 2.8	Rotary Engine, NLF-0416, Single-Slotted Full Span Flap $C_{L_{max}}$ = 3.2	Rotary Engine, NLF-0416, Double-Slotted 0.75 Span Flap $C_{L_{max}}$ = 2.93	Rotary Engine, NLF-0416, Double-Slotted Full Span Flap $C_{L_{max}}$ = 3.35
Stall Speed for W/S = 50 psf, AR = 12		75.4 kt	72.6 kt	67.9 kt	71.0 kt	66.4 kt
Wing Loading Limit for 61 kt Stall		32.8 psf	35.3 psf	40.3 psf	36.9 psf	42.2 psf
Penalty for Meeting 61 kt Stall Requirement	Fuel Used	+14%	+6.9%	+2.4%	+6.4%	+1.5%
	Gross Weight	+8.4%	+6.0%	+1.5%	+4.6%	+1.0%
	Engine Size	+13%	+6.7%	+2.5%	+6.3%	+1.5%

0.75 span double-slotted flaps, it may be difficult to maintain a smooth contour of the wing skin when the device is retracted. A step or gap could cause transition to turbulent flow near the nose of the airfoil. With the possibility of reduced wing laminar flow and the increased cost and complexity, leading edge devices were not considered to be worthwhile for these designs. Even if complete laminar flow could be maintained, the gain in fuel efficiency is only one or two percent for the double-slotted flap system with a leading edge device. The loss in fuel efficiency if laminar flow is not maintained could be as much as 14%.

Composite Materials

The use of advanced fiber composites can reduce aircraft structural weight considerably, resulting in significant fuel savings.

Composite material systems that have been used in aircraft applications include various epoxy matrices reinforced with fiberglass, graphite fibers, boron fibers, and Kevlar.

Fiberglass/epoxy has been used for primary structure in sailplanes for a number of years. Other applications in FAA certified aircraft include helicopter rotors. The primary advantages of fiberglass composites are that they produce very smooth exterior surfaces; they are resistant to fatigue; they have a high damage tolerance; and they allow relatively easy construction, especially with complex curvatures. The use of fiberglass composites does not normally provide a significant weight advantage over aluminum construction.

Boron/epoxy structures are in service in a number of applications, including 33 experimental F-15 empennages. This material has excellent properties but is still too expensive for most commercial uses.

Kevlar, a synthetic aramid fiber made by DuPont, has a very high specific tensile strength and stiffness but fails at relatively low stress levels in compression. Thus, Kevlar composites may be more suited for stiffness-limited components such as fairings and possible fuselage structures. Kevlar composites have much better impact absorption characteristics than graphite or boron composites. Current applications include fairings, helicopter fuselages, some control surfaces, and wing leading edges for the Lear Fan aircraft. Kevlar is intermediate in cost between fiberglass and graphite composites.

Graphite/epoxy (Gr/Ep) is the most promising system for primary structure applications in civil aircraft. A number of commercial aircraft components made of graphite/epoxy have been flown for service testing, including Boeing 737 spoilers. The Boeing 757 and 767 will be produced with Gr/Ep control surfaces. The McDonnell-Douglas AV-8B Harrier utilizes a wing made of Gr/Ep. Finally, the Lear Fan, an aircraft similar to the baseline for this study, is made almost entirely of Gr/Ep.

Weight savings for Gr/Ep structural designs reported in the literature vary widely, from 20 to 40%. Weight savings for components designed to substitute for the 727 elevator, DC-10 rudder, L-1011 aileron, 737 horizontal stabilizer, DC-10 vertical fin, and L-1011 vertical fin in the NASA Aircraft Energy Efficiency program average 25.7% (Reference 20). The composite (Gr/Ep) forward fuselage structure of the AV-8B is 25.3% lighter than an equivalent metal structure (Reference 21). A comparison of the Lear Fan with the Piper Cheyenne, aircraft performing rougly similar missions, indicates that the structural weight saving for the Lear Fan is about 25%. The Lear Fan is conservatively designed to a +6g limit load factor in order to obtain FAA certification and leave some margin for

uncertainties in material properties and environmental effects.

The effects of structural weight reductions of 20, 25, and 30% were investigated using GASP. Table 11 presents the characteristics for these airframes with the advanced diesel engine, compared with the same airframe and engine using conventional structural materials.

The fuselage, wing, and tail structures to which the weight savings are applied make up about 35% of the aircraft empty weight for the advanced diesel airplane, and about 29% of the total gross weight. The reduction in total gross weight is therefore considerably less than the reduction in structural weight.

Questions about the use of composites in primary structure related to moisture absorption, lightning strike protection, crashworthiness, and manufacturing costs are rapidly being answered. As the technology of manufacturing composite airframes matures, they may become less costly than conventional construction. It is also anticipated that somewhat greater weight savings may be achieved as experience with composites increases.

Canard Configuration

Most conventional configurations fly with a download on the tail, requiring an increase in lift on the main wing and causing trim drag. The use of a canard configuration, where both surfaces produce lift, would appear to allow a reduction in trim drag.

The downwash/upwash field from the canard can considerably affect the aft wing. At cruise, with a canard of shorter span than the wing, the inboard main wing section will be in downwash, while the outboard section will experience upwash. Twisting the wing tip sections down

Table 11 Comparison of Conventional Aluminum and Composite Airplanes with Pusher Engines, Laminar Wing, Advanced Diesel Engine--Baseline Mission Performance

	Wing Loading psf	Aspect Ratio	Gross Weight, lb.	Change in Gross Weight	Fuel Used, lb	Fuel Saved	Average Cruise Specific Range, nm/lb.	Change in Engine Size
Conventional Structure	50	12	4458	-	461	-	3.21	-
-20% ΔW Composite Airframe	50	12	4144	-7%	444	3.7%	3.32	-4.7%
-25% ΔW Composite	50	12	4061	-8.9%	440	4.6%	3.35	-5.8%
-30% ΔW Composite	50	12	3990	-10.5%	435	5.6%	3.38	-7.4%

relative to the root can help equalize the wing lift distribution, and result in a thrust component sufficient to offset the drag caused by the downwash field.

A canard configuration was analyzed based on a main wing aspect ratio of 12 and a pusher engine. The passenger cabin for the canard design is identical to that of the baseline design. Detailed weight and balance and aerodynamic center calculations were not performed, but minor adjustments in wing location and sweep should produce a viable configuration.

The change in center of gravity location as fuel is burned can be a problem with canard designs if fuel is carried in the wing only. Use of fuselage or wing strake fuel tanks may be necessary. Fuselage fuel tanks can be acceptable from a safety standpoint if measures used in military aircraft and helicopters are adopted, such as nylon reinforced fuel bladders.

Trim change with wing flap deflection may also be a problem if the wing is relatively far aft of the aircraft center of gravity. Minimizing the canard area to wing area ratio alleviates this problem. A canard/wing area ratio of 0.25 was chosen for this design.

A main wing aspect ratio of 12 was chosen for comparison with the advanced baseline. A canard aspect ratio of 8.0 was chosen to keep the canard chord reasonable.

A computer program using the Quasi Vortex Lattice Method of Lan[24] was used to compare induced drag values for the canard and conventional configurations at angles of attack representative of climb and cruise. Reference area for the canard design is the total lifting area (wing area

plus canard area). This facilitates the use of GASP to analyze a canard design. Figure 12 shows the induced drag values calculated by QVLM as a function of lift coefficient for the two configurations at various angles of attack and Mach numbers. The induced drag of the canard design is considerably higher than that of the conventional design. Assuming that both designs have the same Oswald efficiency factor, the effective aspect ratio for the canard design is 7.9 in cruise.

GASP was not designed to analyze unconventional configurations, but a close approximation to a canard is possible. Using the total lifting area as the reference area, it is necessary to set the horizontal tail size input to a negligible value. Aspect ratio is set to the effective aspect ratio for the total configuration, 7.9. Normal fuselage geometry is used. This results in an airplane with less wetted area due to the shorter fuselage and elimination of the horizontal tail.

Table 12 compares the performance of a diesel engine pusher canard design with composite structure to a conventional configuration also utilizing composites.

Table 12 Comparison of Canard and Conventional Configurations with Diesel Pusher Engine and Composite Structure

	Gross Weight, lb	Cruise Specific Range, lb	Fuel Used, lb	Engine Size, hp
Canard	3798	3.49	421	1055
Conventional	4061	3.35	440	1100
Improvement due to canard	-6%	+4%	-4%	-4%

The differences in wetted areas and fuselage weight more than make up for the less favorable induced drag of the canard design in this case.

The induced drag of the canard design could probably be improved by optimizing the canard location and size relative to the wing.

MISSION TRADE ANALYSIS

The baseline mission (Table 1) selected for this study is somewhat arbitrary. Nevertheless, it was defined with specific objectives in mind. The cruise speed of 300 knots is near the practical upper limit for propeller-driven airplanes. The range of 1300 nm is comparable with that of most twin-engine piston and turboprop airplanes available today and is a significant improvement over virtually all current single engine airplanes (see Figure 1).

It is desirable, however, to assess the sensitivity of the airplane performance parameters and configuration to changes in the mission speed, range, and payload. The following sections present data that resulted from such a study.

Effect of Cruise Speed

To determine the effect of cruise speed, the airplane was sized to the baseline mission except that cruise speeds were set at 200, 250, 300, and 350 knots. At each speed, variations were made in wing loading and aspect ratio to determine optimum fuel efficiency. This was done for each of the four propulsion systems described in the previous section.

The effect of cruise speed is summarized in Figure 13, which shows the effect of cruise speed on total fuel, specific range during cruise, and takeoff gross weight. These data represent optimum values of wing loading at each speed with aspect ratio of 12.

It is clear that an increase in cruise speed exacts a penalty in fuel efficiency and gross weight. For example, a 50 percent increase in cruise speed, from 200 to 300 knots, results in a 20 to 30 percent increase in total fuel used for the 1300 nm mission, and a 16 to 23 percent reduction in cruise specific range. The corresponding increase in gross weight is less than 100 lb (about 2.5 percent).

Effect of Range

The airplane was sized for range performance varying from 900 to 1700 nm. All other baseline mission requirements were held constant. The results are presented in Figure 14 for each of the four propulsion systems, using an aspect ratio of 12 and optimum wing loading. A 31% (400 nm) change in range requirement from the nominal 1300 nm results in approximately a 29% change in total fuel and about a 5% change in takeoff gross weight. Specific range during cruise increases as range decreases by almost exactly the percent decrease in gross weight.

Effect of Payload

A study of the effect of payload on gross weight and fuel consumption was conducted by sizing airplanes with four different propulsion systems to the basic mission, except for payload which was varied over the range from 800 to 1600 lb. Results are presented in Figure 15 for airplanes with optimum wing loading and aspect ratio of 10.

Fuel required for the mission is almost a linear function of payload. A 1.0 lb change in payload results in approximately a 0.15 lb change in fuel required. Cruise specific range changes from 9% to 15% for a 50% change in payload, and gross weight increases about 1.67 to 2.0 lb per lb of payload, depending on engine type.

INTEGRATED DESIGN

In order to determine the maximum potential benefits from the synergistic combination of all advanced technologies considered in this study, an advanced technology configuration with the following characteristics was analyzed:

- rotary engine
- pusher propeller
- laminar wing
- laminar flow on forward fuselage
- composite materials with 25% structural weight reduction
- conventional wing-tail configuration

The canard was not employed because of the limitations of GASP in producing an accurate canard analysis.

The results are presented in Table 13. Performance and configuration improvements relative to the baseline and current production aircraft are extremely large. The gross weight is 33% less than the baseline airplane (Table 3) and the total fuel has been reduced to 43.7% of that used by the baseline airplane.

Figure 16 underscores the dramatic advances that are possible in fuel efficiency and performance through the application of advanced technology. The integrated design achieves four times the specific range of current turboprops with comparable speed, or doubles the specific range (and total range) of the best current single-engine piston airplanes while increasing cruise speed by 100 knots.

Table 13 Advanced Integrated Configuration Summary
Pusher Rotary Engine, Laminar Flow, Composite Structure

Configuration Data:	
gross weight	3690 lb
wing area	73.8 ft^2
wing loading	50
aspect ratio	12
wing fuel volume	72.5 gal
empty weight	2050 lb
maximum payload	1200 lb
engine	Rotary
sea level max. power	581 hp
propulsion system weight	657 lb
Performance:	
cruise speed	297.8 kt
cruise altitude	35,000 ft
range (max. payload)	1300 nm
average cruise specific range	3.34
total fuel for max. payload mission	433 lb
range (max. fuel)	1300 nm
takeoff distance to 50 ft	2112 ft
landing distance from 50 ft	1309 ft
stall speed (takeoff, max. gross weight)	76.2 kt
stall speed (landing, max. gross weight)	64.7 kt
stall speed (landing, end of mission)	60.8 kit
L/D_{max}	18.16
L/D_{cruise}	16.13

CONCLUSIONS

The potential exists to greatly improve the fuel efficiency and mission capability of single-engine airplanes through the application of advanced technology to engines, aerodynamic design, and materials.

The turbine engine, while being very light weight, cannot match advanced internal combustion engines in fuel economy for this mission. Its relatively high cost may also be a deterring factor.

The other three engines considered have very nearly equal fuel performance, but the rotary engine produces the lightest and smallest airplane. Other attractive features of the rotary are its relatively small size, competitive cost, multifuel capability, and simplicity. The low lapse rate, which results in a low maximum power rating, depends on advancements in the technology of turbochargers. However, the SIR engine has the benefit of tradition, operational experience, and customer acceptance.

To take full advantage of technologies that can reduce fuel consumption, some modification to the FAR rule requiring a stall speed less than 61 knots will be needed.

Laminar flow wings, combined with composite structural materials offer considerable promise for improved performance and fuel efficiency.

With vigorous development of the technologies discussed herein, significant improvements can be achieved in the performance, efficiency, and utility of general aviation aircraft during the next decade.

REFERENCES

[1]"Federal Aviation Administration Aviation Forecasts Fiscal Years 1981-1982", September 1980.

[2]Bruce J. Holmes, "Aerodynamic Design Optimization of a Fuel Efficient High-Performance Single-Engine Business Airplane." AIAA Paper No. 80-1846, 1980.

[3]David L. Kohlman; Garey T. Matsuyama, Kevin E. Hawley, and Paul T. Meredith, "A Feasibility Study for Advanced Technology Integration for General Aviation." NASA CR 159381, 1980.

[4]T. J. Wickenheiser, G. Knip, R. M. Plencner, and W. C. Strack, "Comparisons of Four Alternative Powerplant Types for Future General Aviation Aircraft." NASA TM 81584, 1980.

[5]Holmes, Bruce J.; and Croom, Cynthia C.: "Aerodynamic Design Data for a Cruise-Matched High Performance Single-Engine Airplane." SAE paper 810625, April 1981.

[6]"GASP - General Aviation Synthesis Program." NASA CR 152303, prepared by Aerophysics Research Corp., January 1978.

[7]David L. Kohlman, "Flight Test Results for an Advanced Technology Light Airplane." Journal of Aircraft, Vol. 16, April 1979, pp. 250-255.

[8]Bruce J. Holmes, "Flight Evaluation of an Advanced Technology Light Twin-Engine Airplane (ATLIT)." NASA CR-2832, July 1977.

[9]Holmes, B. J.; Yip, L. P.: Coy, P. F.; and Obara, C. J.; "Flight and Wind-Tunnel Investigations of Natural Laminar Flow on Modern Airplane Surfaces, " Proposed NASA Technical Paper.

[10]Holmes, Bruce J.; Hoffman, Michael J.; Obara, Clifford J.; and Gregorek, Gerald M.; "Natural Laminar Boundary Layer Flight Test Data on a High Performance Single-Propeller-Driven, Composite Airplane," Proposed NASA Technical Paper.

[11]Holmes, Bruce J.; and Obara, Clifford J.: "Observations and Implications of Natural Laminar Flow on Practical Airplane Surfaces." ICAS paper 82-5.1.1.

[12]Somers, Dan M.: "Design and Experimental Results for a Natural Laminar Flow Airfoil for General Aviation Applications." NASA TP 1861, 1981.

[13]Kohlman, David L.; Schweikhard, W. G.; and Albright, A. E.: "Icing Tunnel Tests of a Clycol-Exuding Porous Leading Edge Ice Protection System on a General Aviation Airfoil." NASA CR 165444, 1981.

[14]Lockheed-Georgia Co.: "Evaluation of Laminar Flow Control System Concepts for Subsonic Commercial Transport Aircraft." NASA CR 159253, 1980.

[15]Peterson, John B. Jr.; and Fisher, David F.: "Flight Investigation of Insect Contamination and Its Alleviation." NASA CP 2036, 1978.

[16]NASA Four Engine Study Master Data Chart, March 17, 1981 (furnished by NASA Lewis Research Center).

[17]"General Aviation Propulsion," proceedings of NASA Lewis conference. NASA CP-2126, November 1979.

[18]T. J. Wickenheiser, G. Knip, R. M. Plencner, and W. C. Strack, "Comparisons of Four Alternative Powerplant Types for Future General Aviation Aircraft." NASA TM 81584, 1980.

[19]A. P. Brouwer, "150 and 300 KW Lightweight Diesel Aircraft Engine Design Study." NASA CR-3260, 1980.

[20]Louis F. Vosteen, "Composite Aircraft Structures"; in "Fibrous Composites in Aircraft Design," proceedings of the Fourth Conference on Fibrous Composites, San Diego, 1978.

[21]James C. Watson, "AV-8B Composite Fuselage Design." J. of Aircraft, Vol. 19, No. 3, March 1982, pp. 235-238.

[22]K. L. Sanders, SAWE Paper 761, SAWE Journal, May 1961.

[23]D. E. Hoak, et al., USAF Stability and Control Datcom. Air Force Flight Development Lab, 1976.

[24]C. E. Lan, "A Quasi-Vortex-Lattice Method in Thin Wing Theory," J. of Aircraft, Vol. 11, September 1974, pp. 518-527.

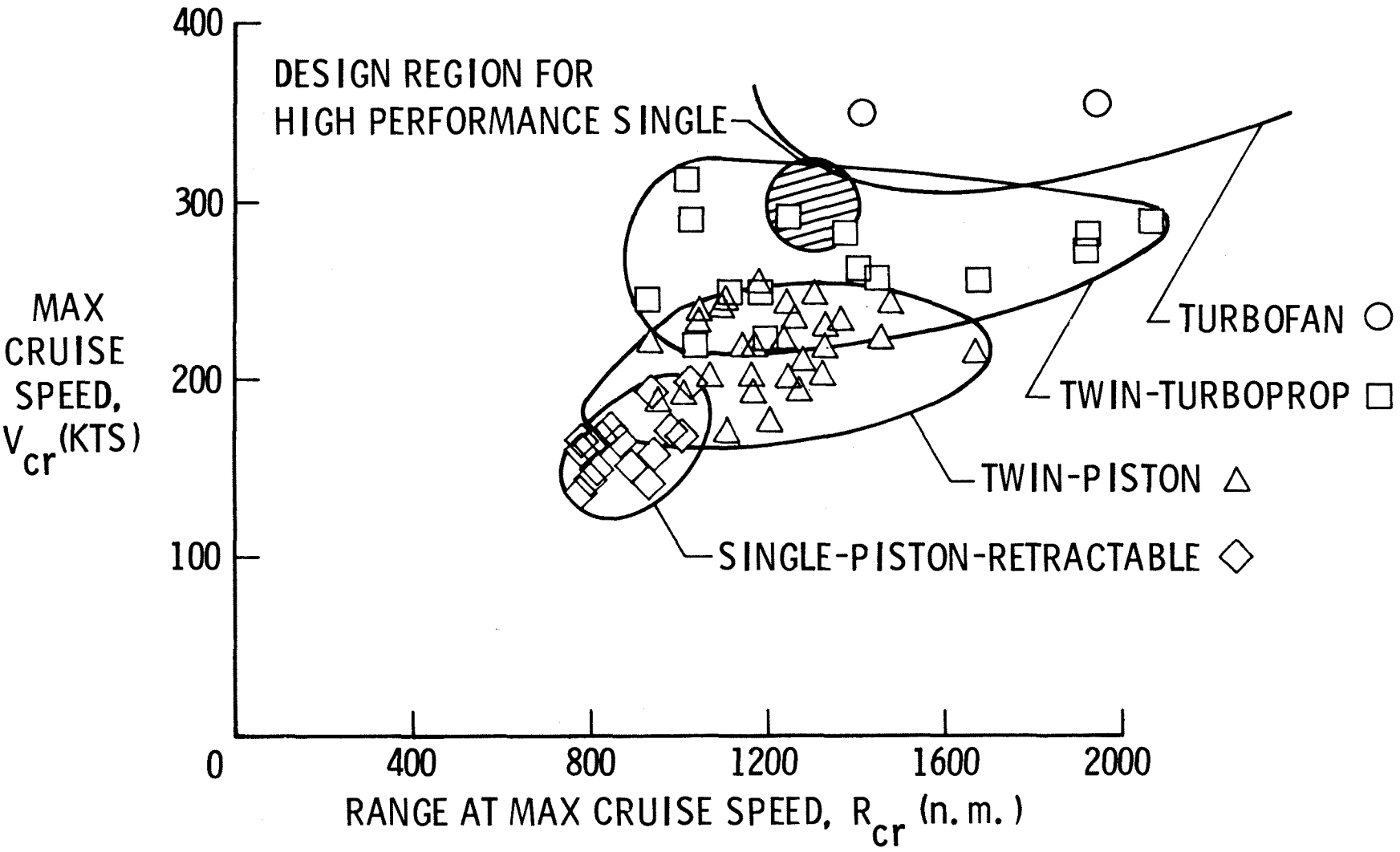

Figure 1. Comparison of High-Performance Single Engine Airplane Performance Goal with Current Production Airplane Performance.

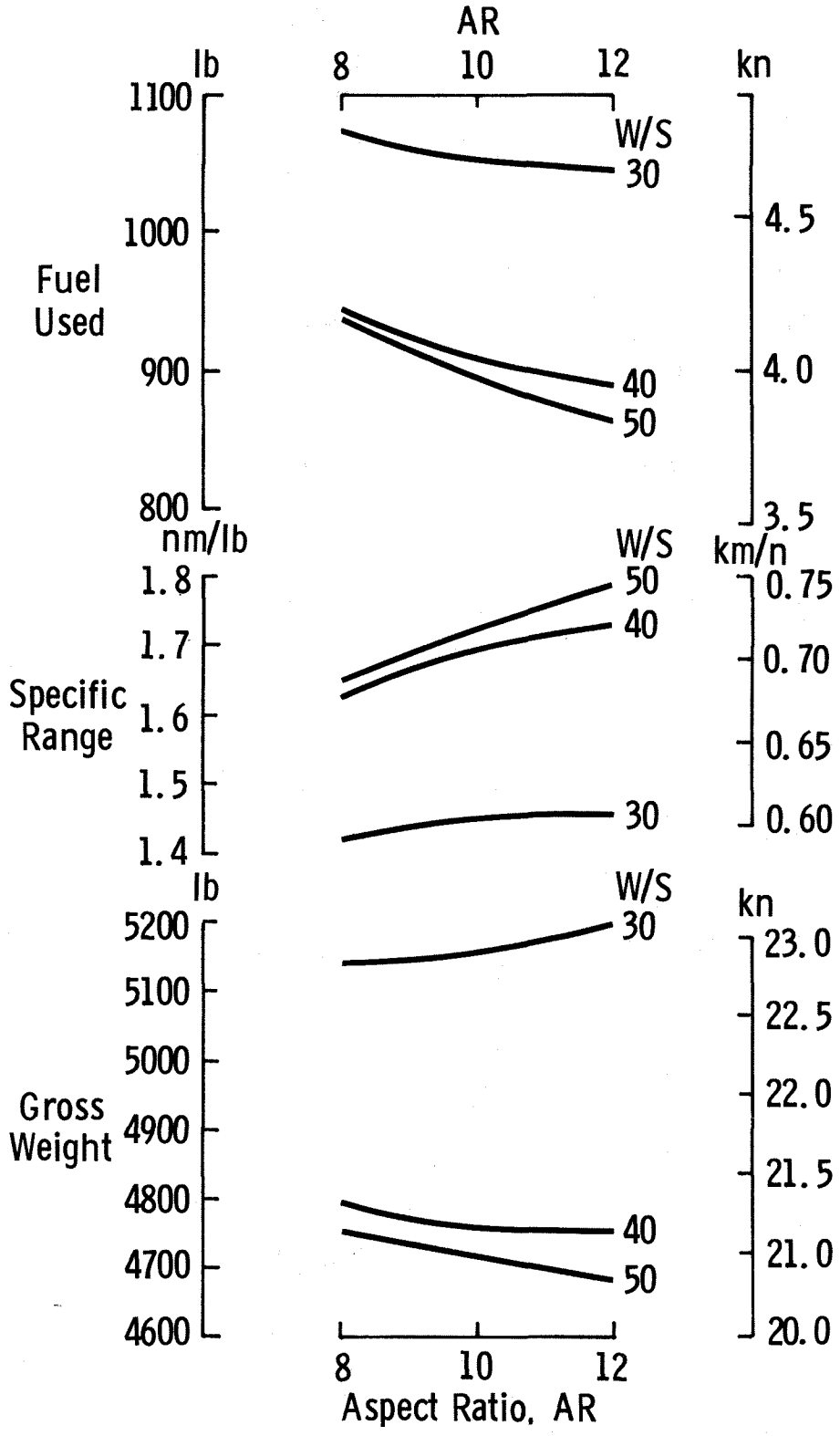

Figure 2. Effect of Aspect Ratio on Baseline Airplane

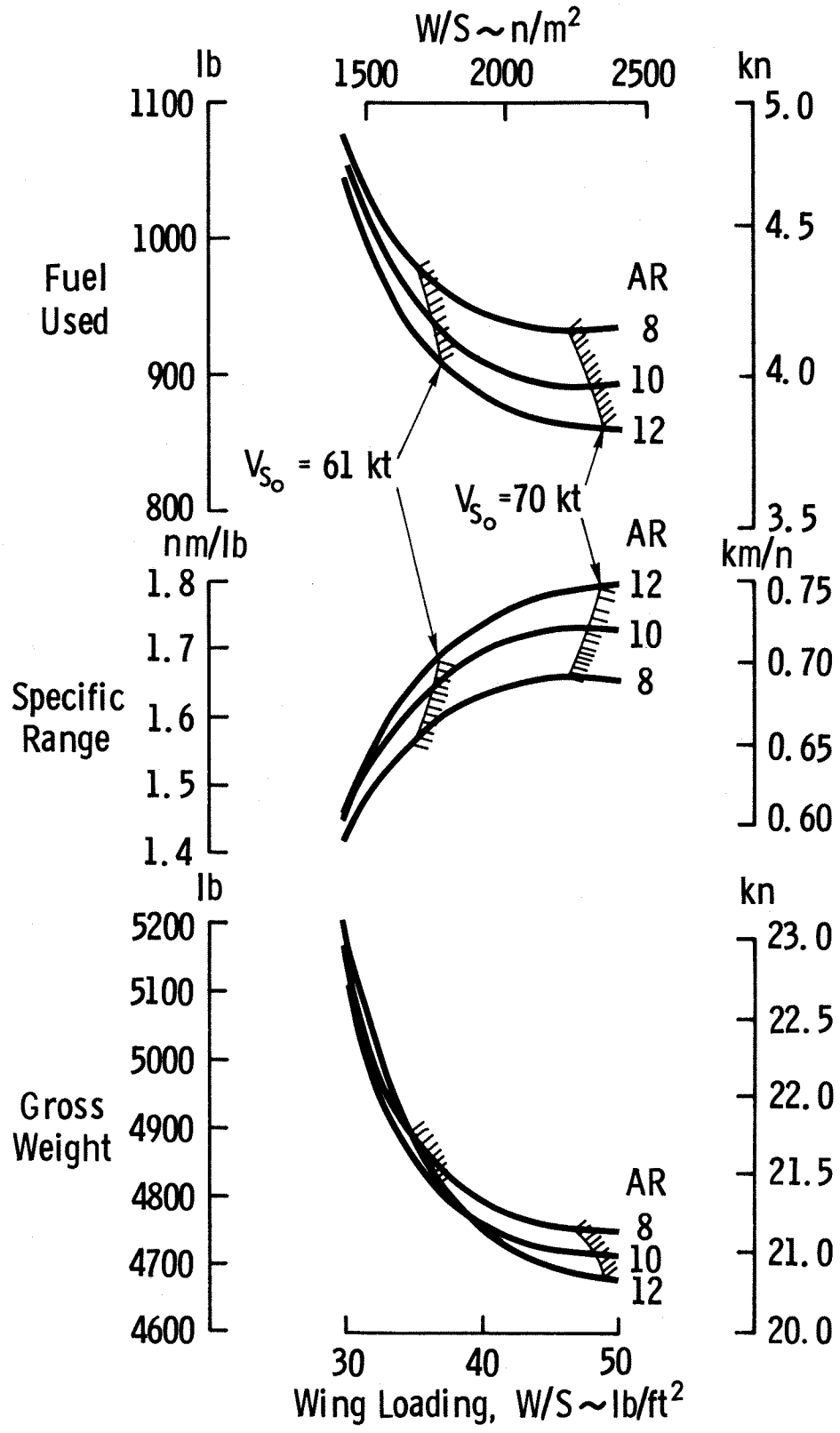

Figure 3. Effect of Wing Loading on Baseline Airplane

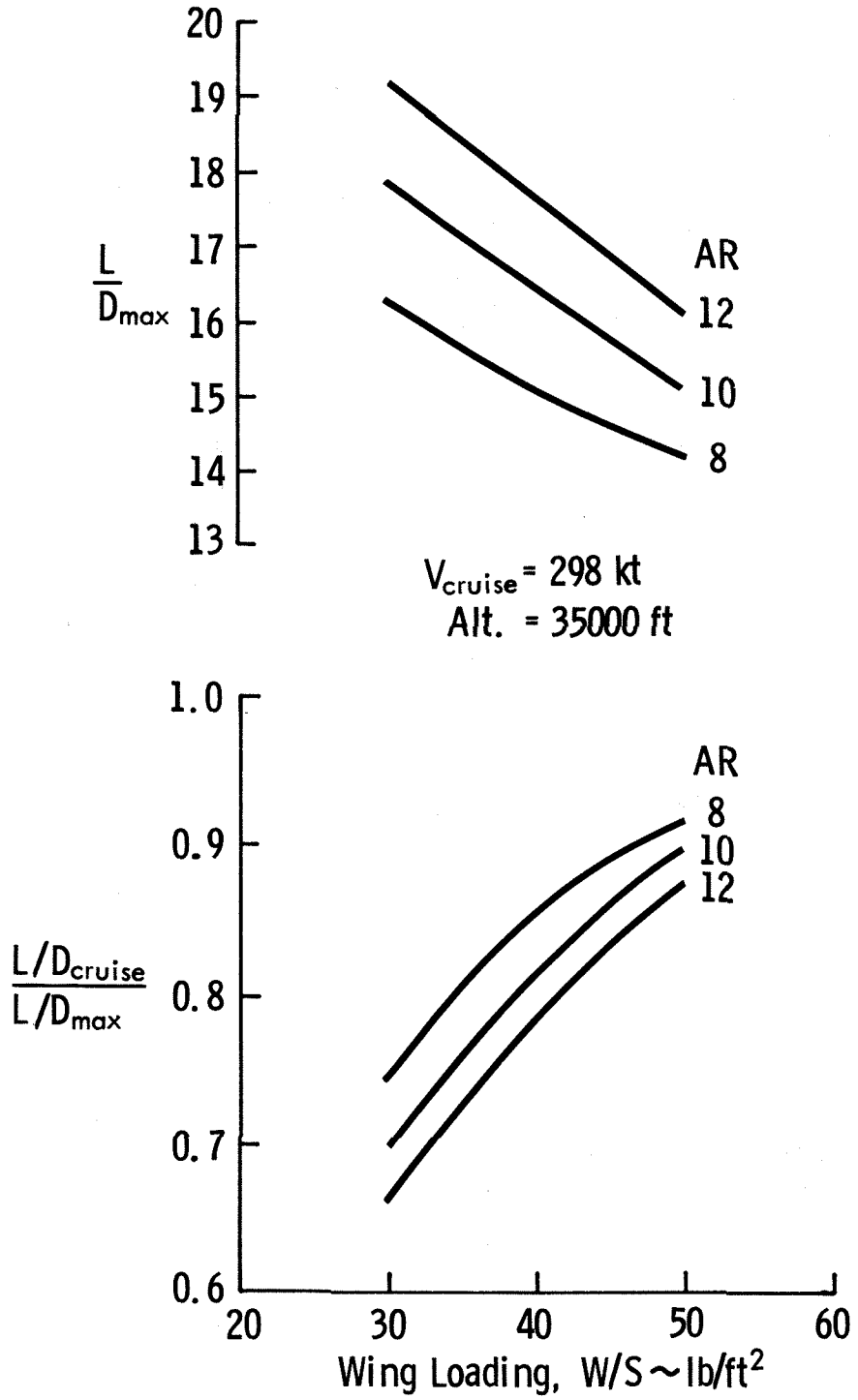

Figure 4. Effect of Wing Loading on (L/D) Max and Cruise Matching Parameter of Baseline Airplane

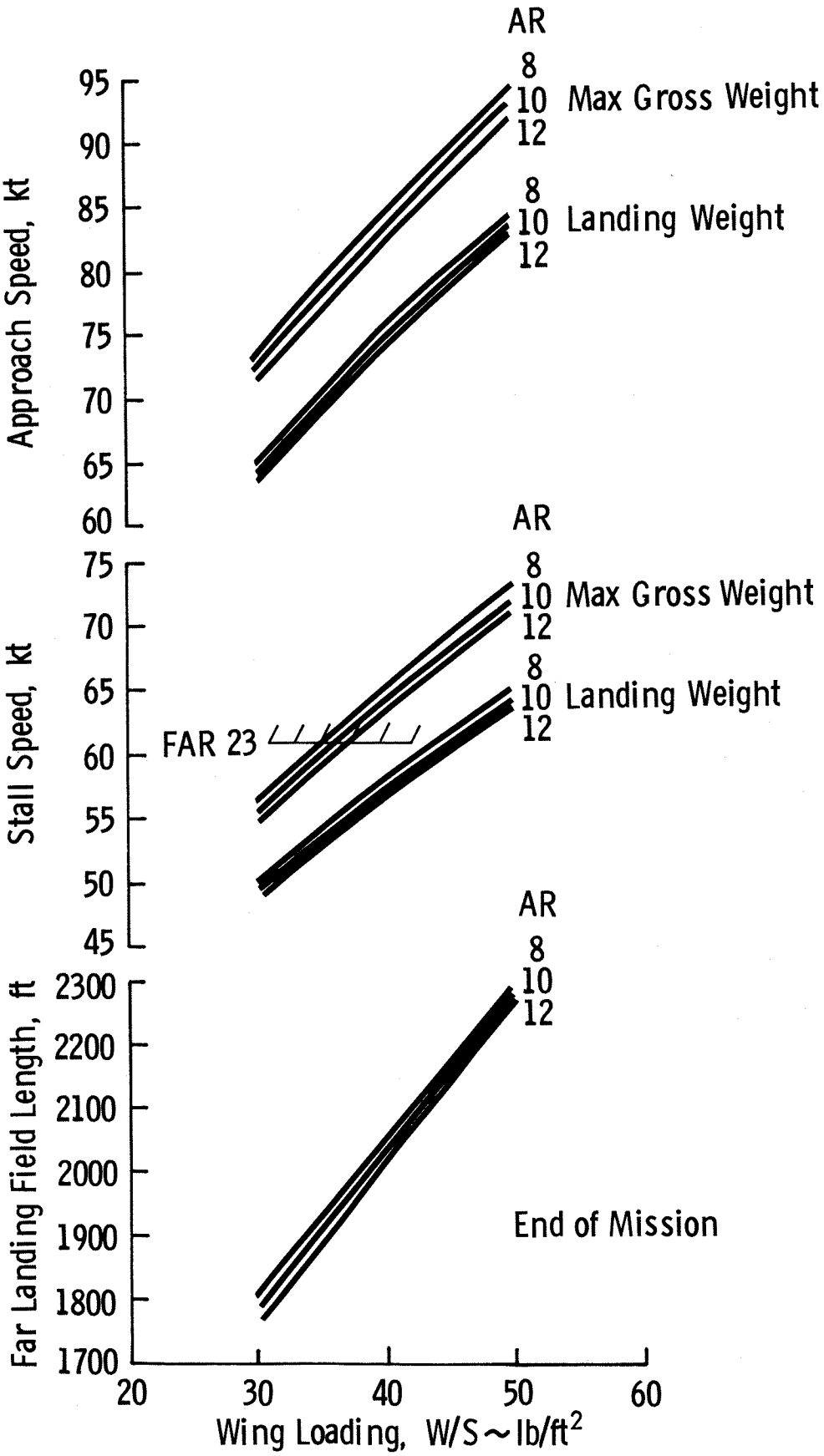

Figure 5. Effect of Wing Loading on Approach Speed, Stall Speed and FAR Landing Field Length of Baseline Airplane

Figure 6. Laminar Flow Visualization on the Bellanca Skyrocket II. $R_x = 1.9 \times 10^6$ ft.$^{-1}$; $C_L = 0.20$ (Reference 10)

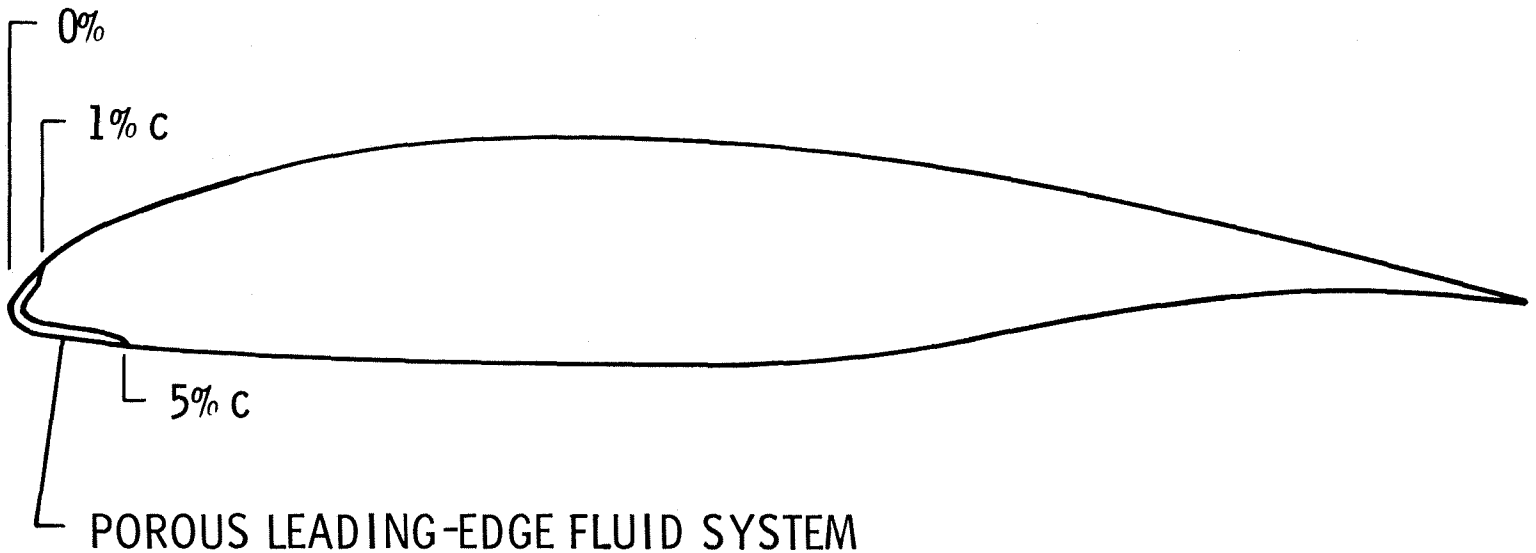

Figure 7. Porous Leading Edge Ice and Insect Protection System for Natural Laminar Flow Wings.

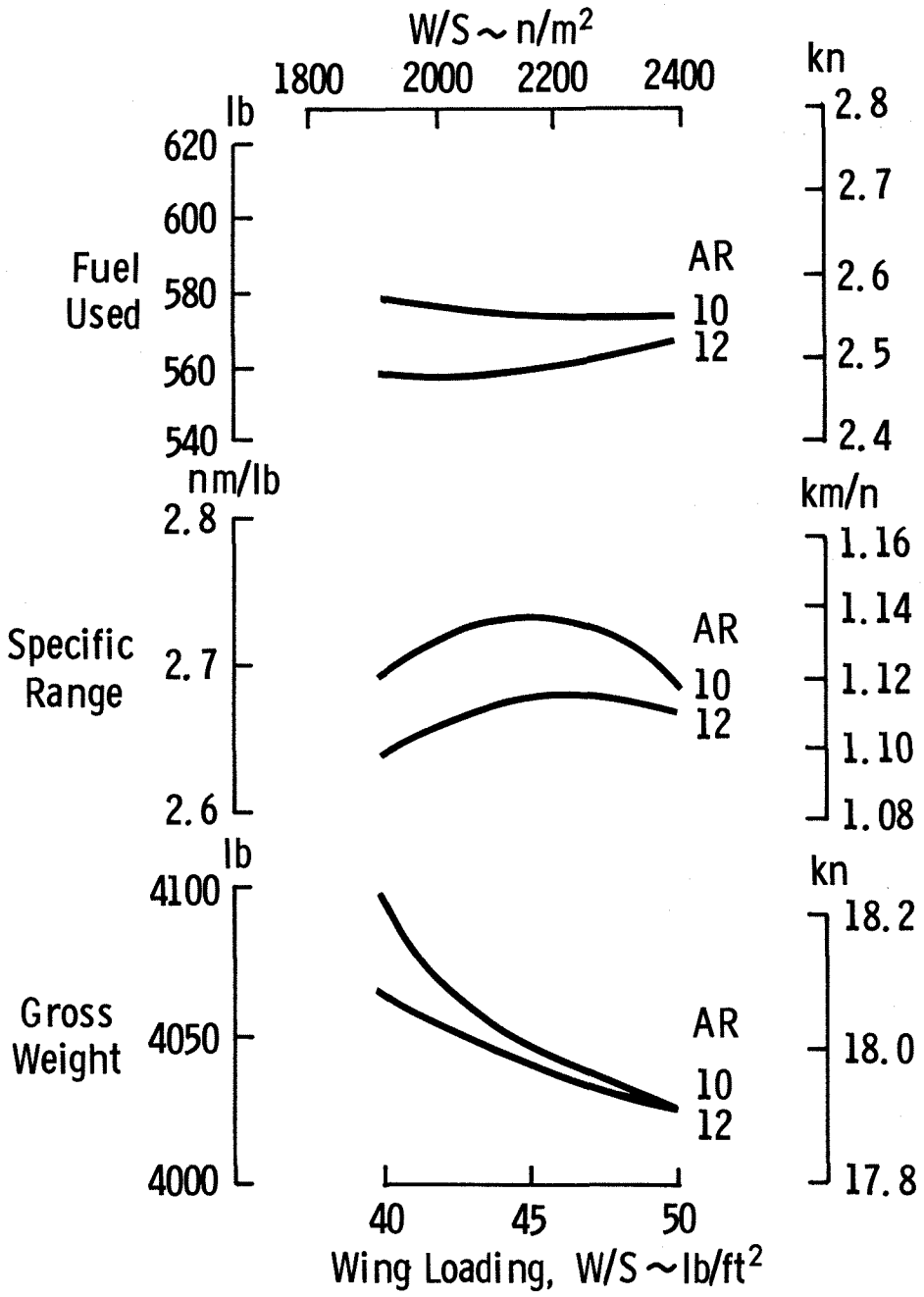

Figure 8. Fuel Requirements and Gross Weight Characteristics of an Advanced Single-Engine Airplane with a GATE Engine

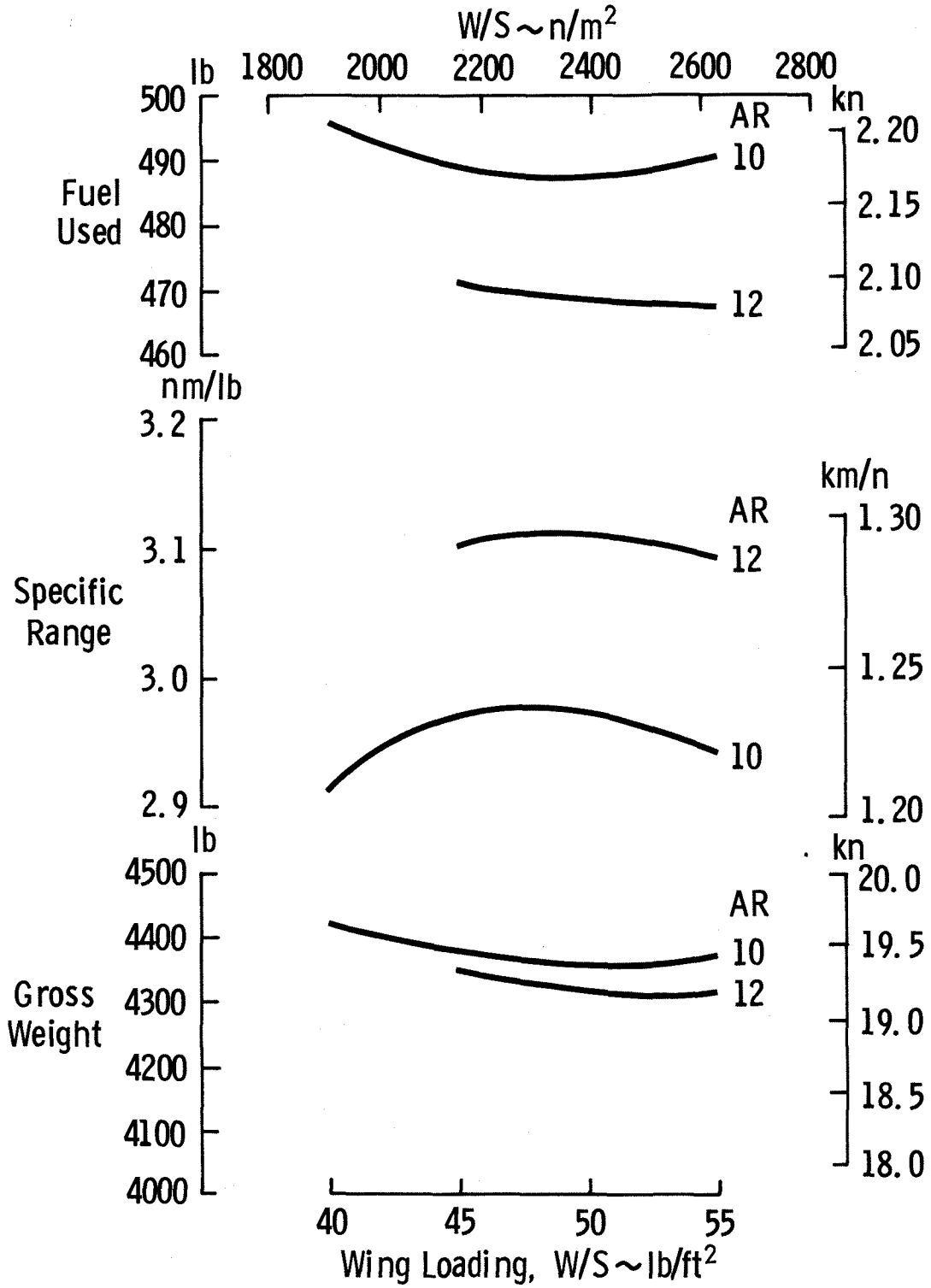

Figure 9. Fuel Requirements and Gross Weight Characteristics of an Advanced Single-Engine Airplane with a SIR Engine

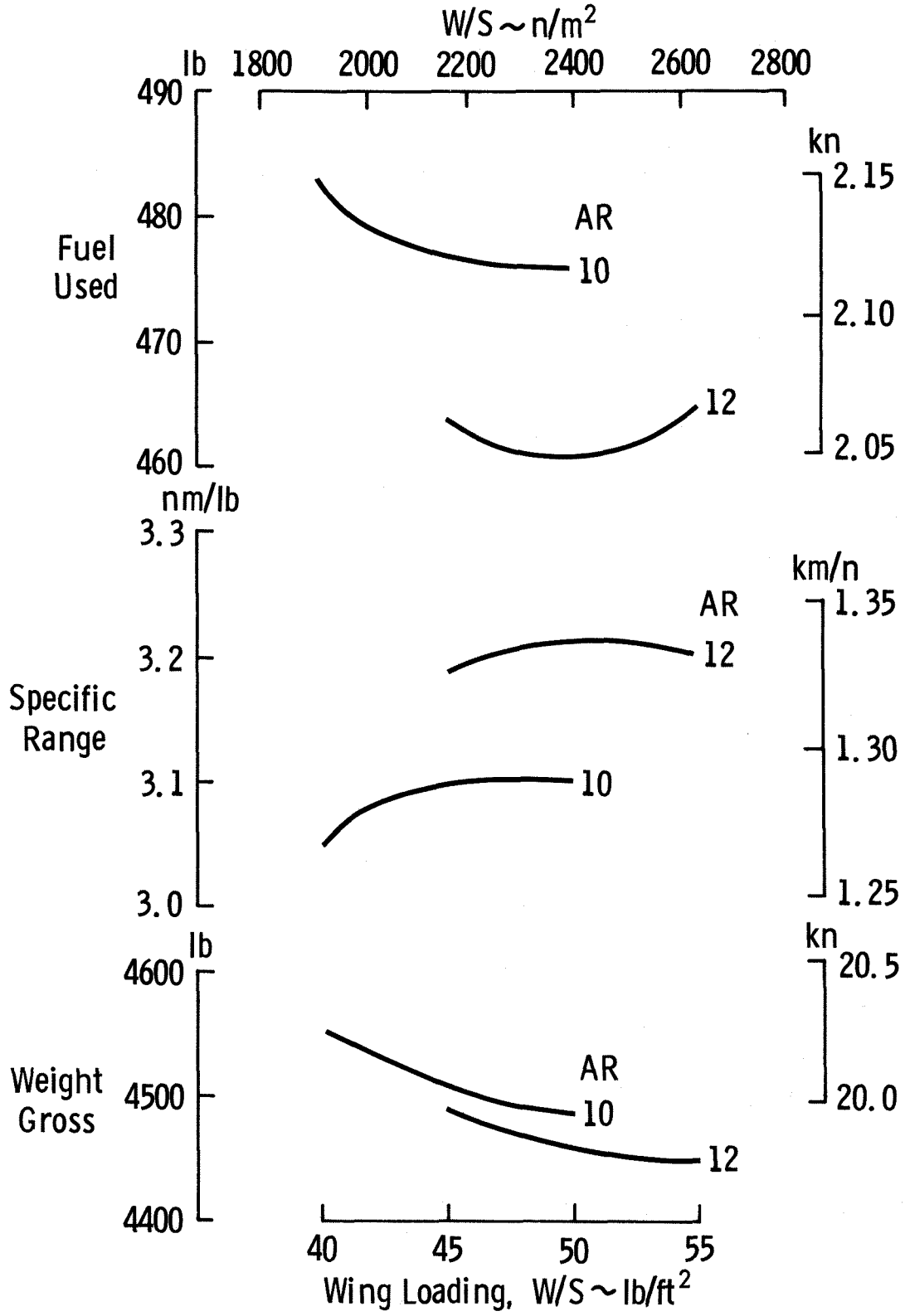

Figure 10. Fuel Requirements and Gross Weight Characteristics of an Advanced Single-Engine Airplane with a Diesel Engine

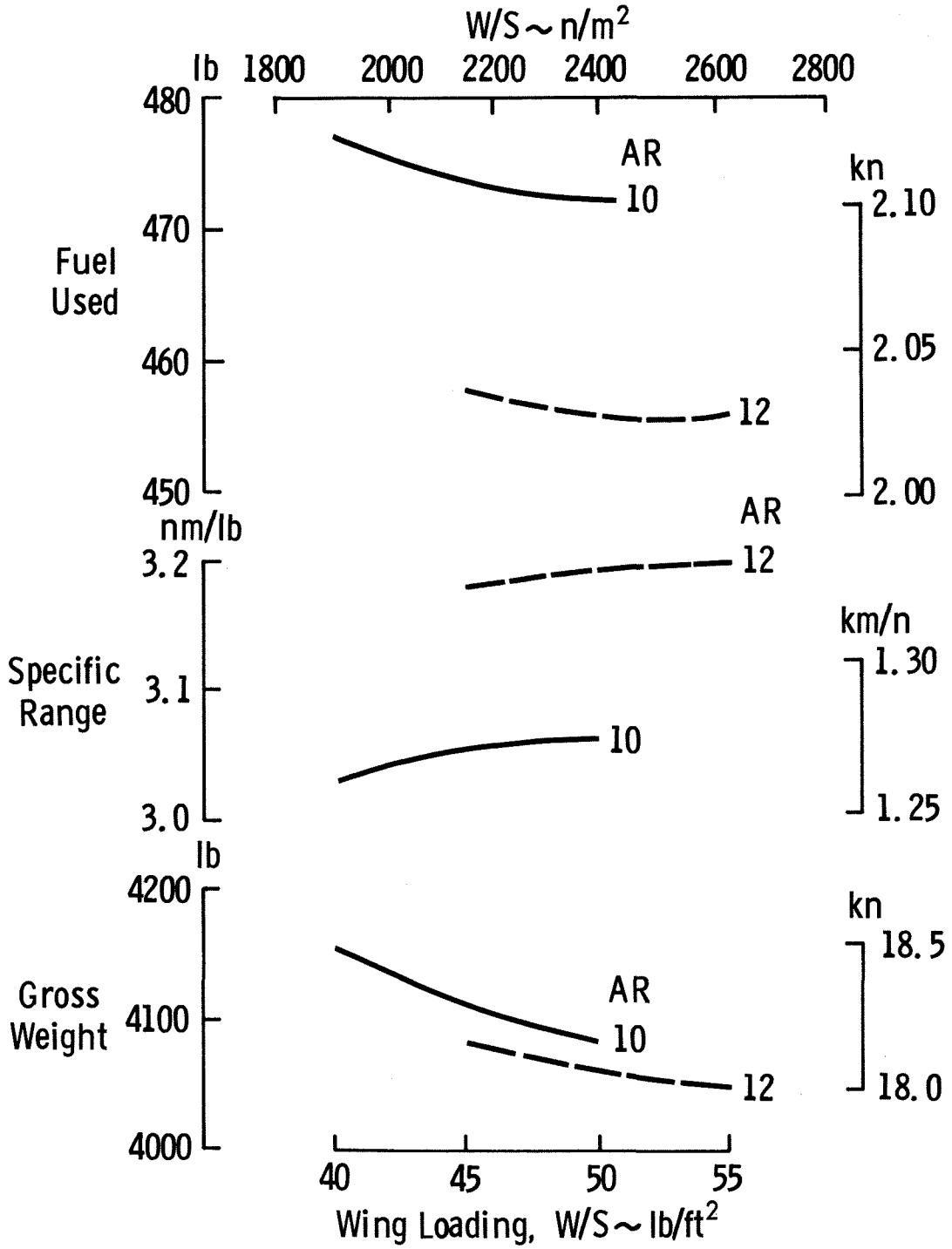

Figure 11. Fuel Requirements and Gross Weight Characteristics of an Advanced Single-Engine Airplane with a Rotary Engine

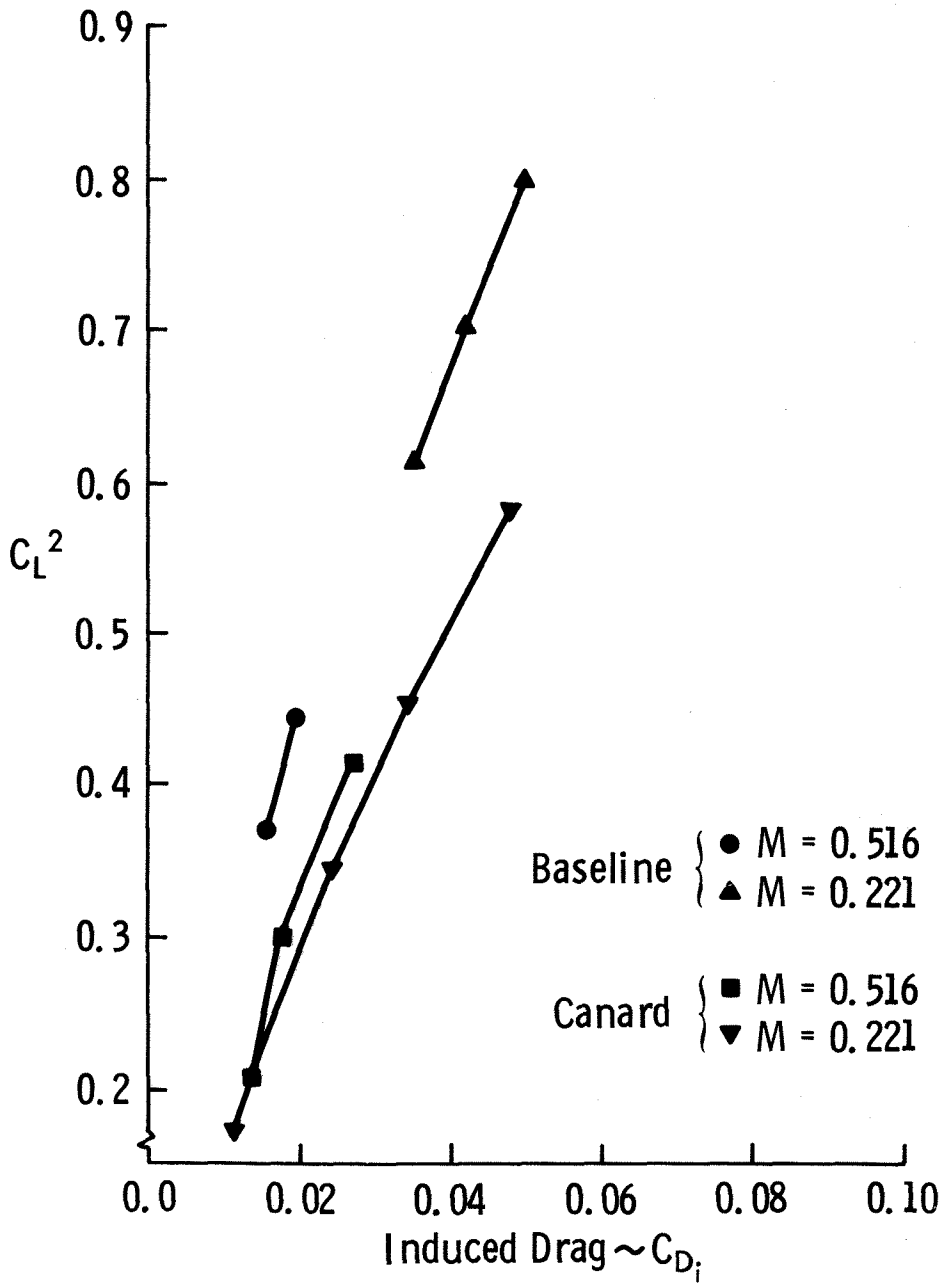

Figure 12. Theoretical Prediction of Induced Drag of a Canard and Conventional Airplane Using QVLM Program

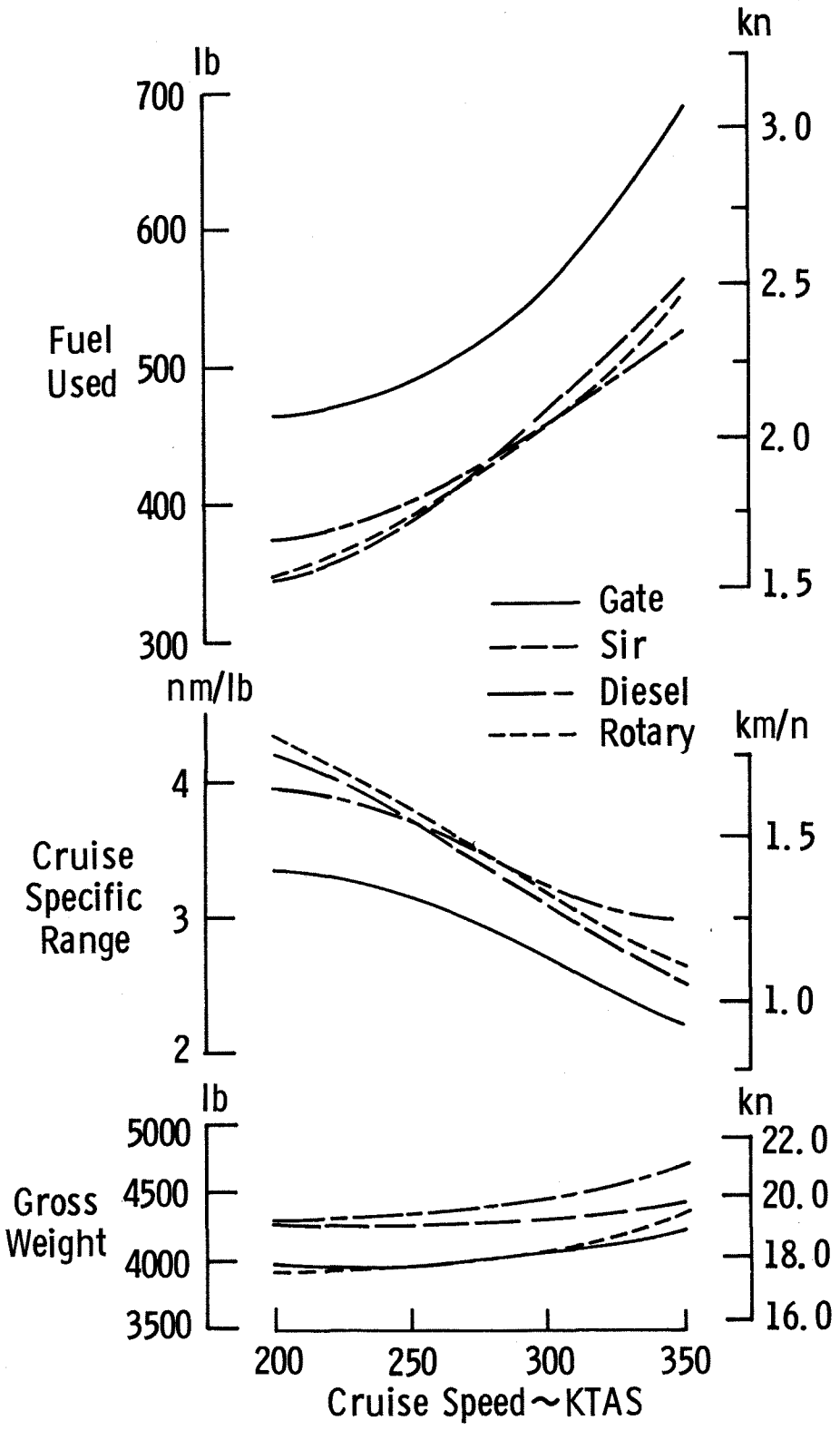

Figure 13. Effect of Cruise Speed. Optimum W/S, AR = 12, Pusher Propeller, Laminar Flow Wing and Fuselage

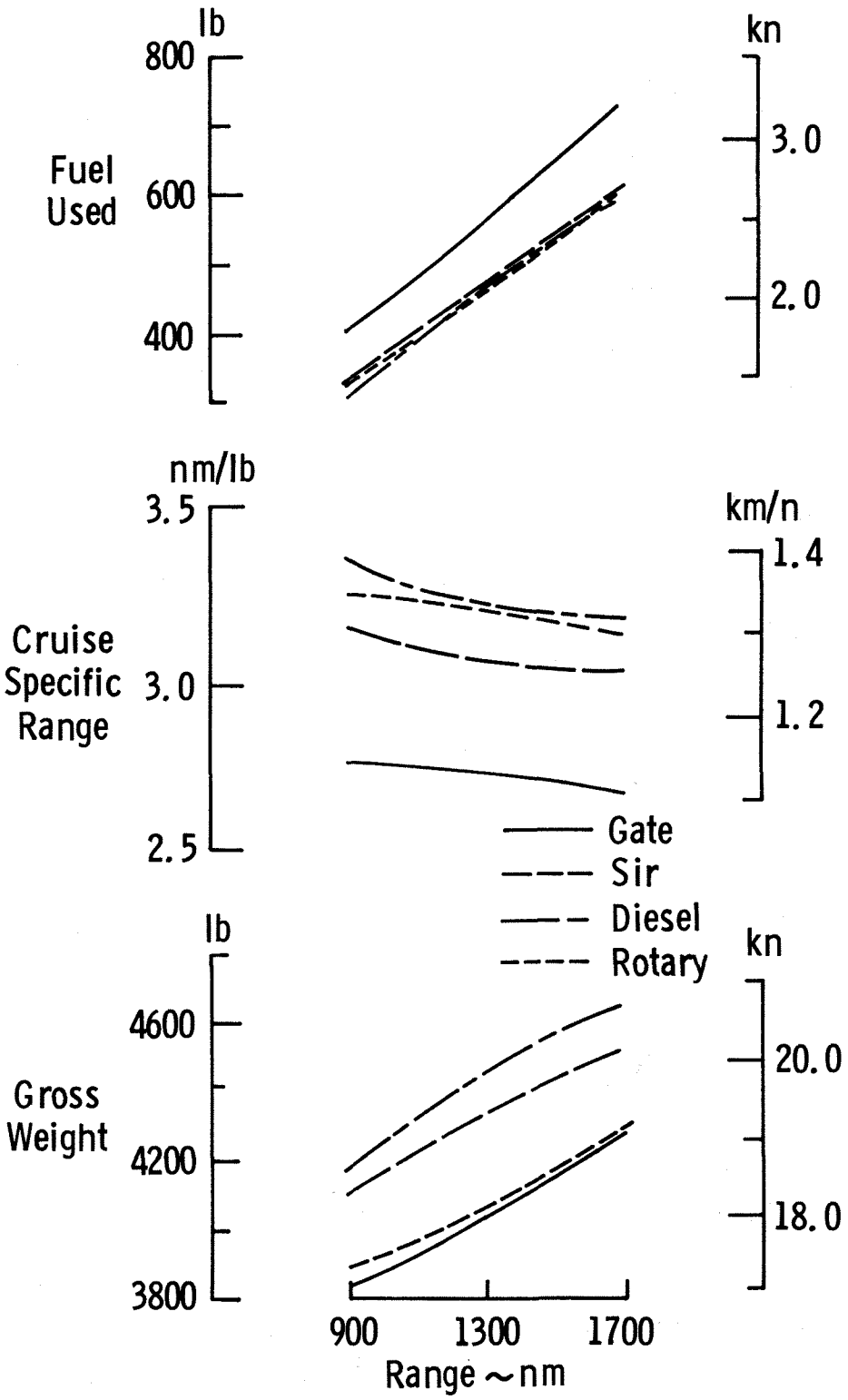

Figure 14. Effect of Range. Optimum W/S, AR = 12, Pusher Propeller, Laminar Flow Wing and Fuselage

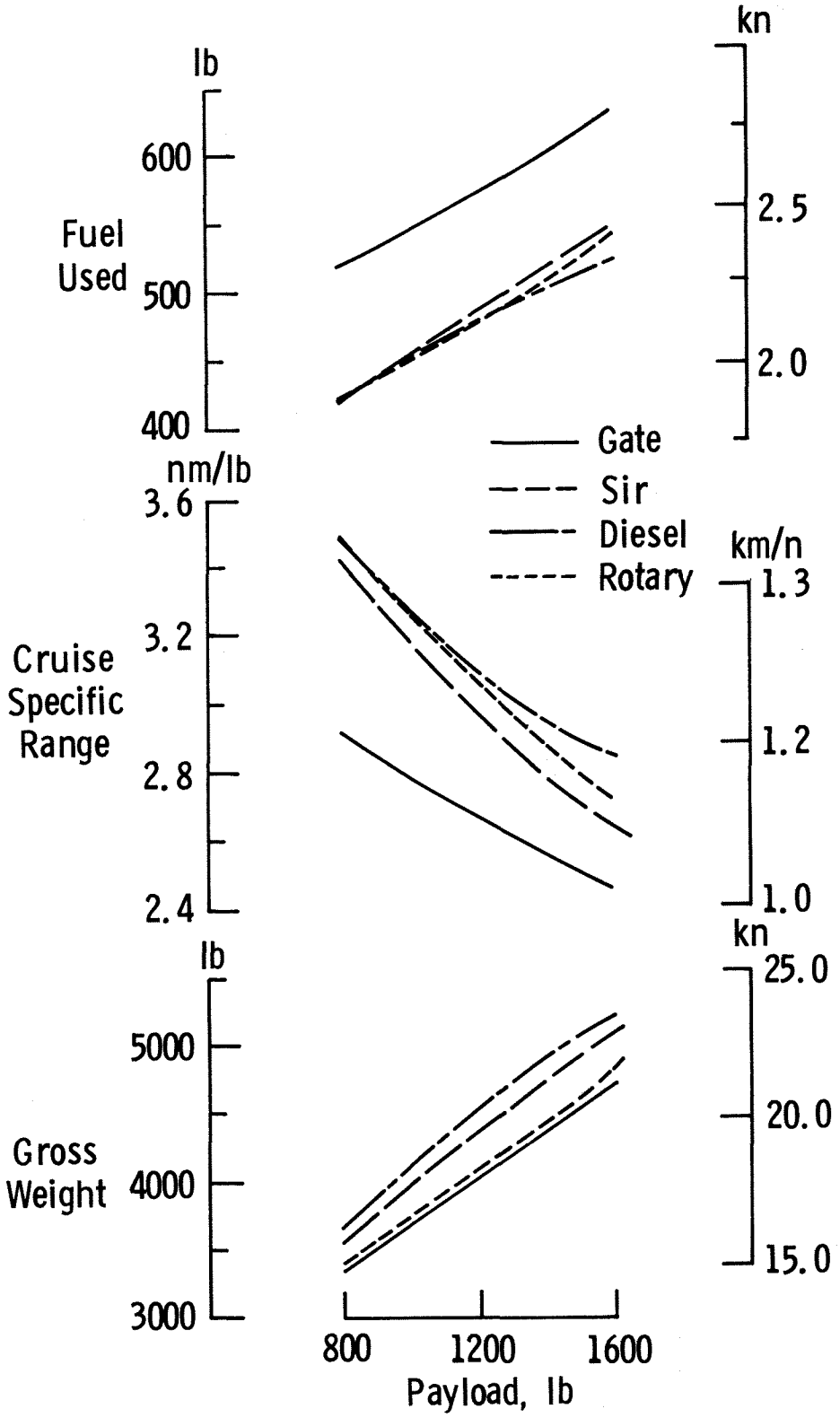

Figure 15. Effect of Payload. Optimum W/S, AR = 12, Pusher Propeller, Laminar Flow Wing and Fuselage

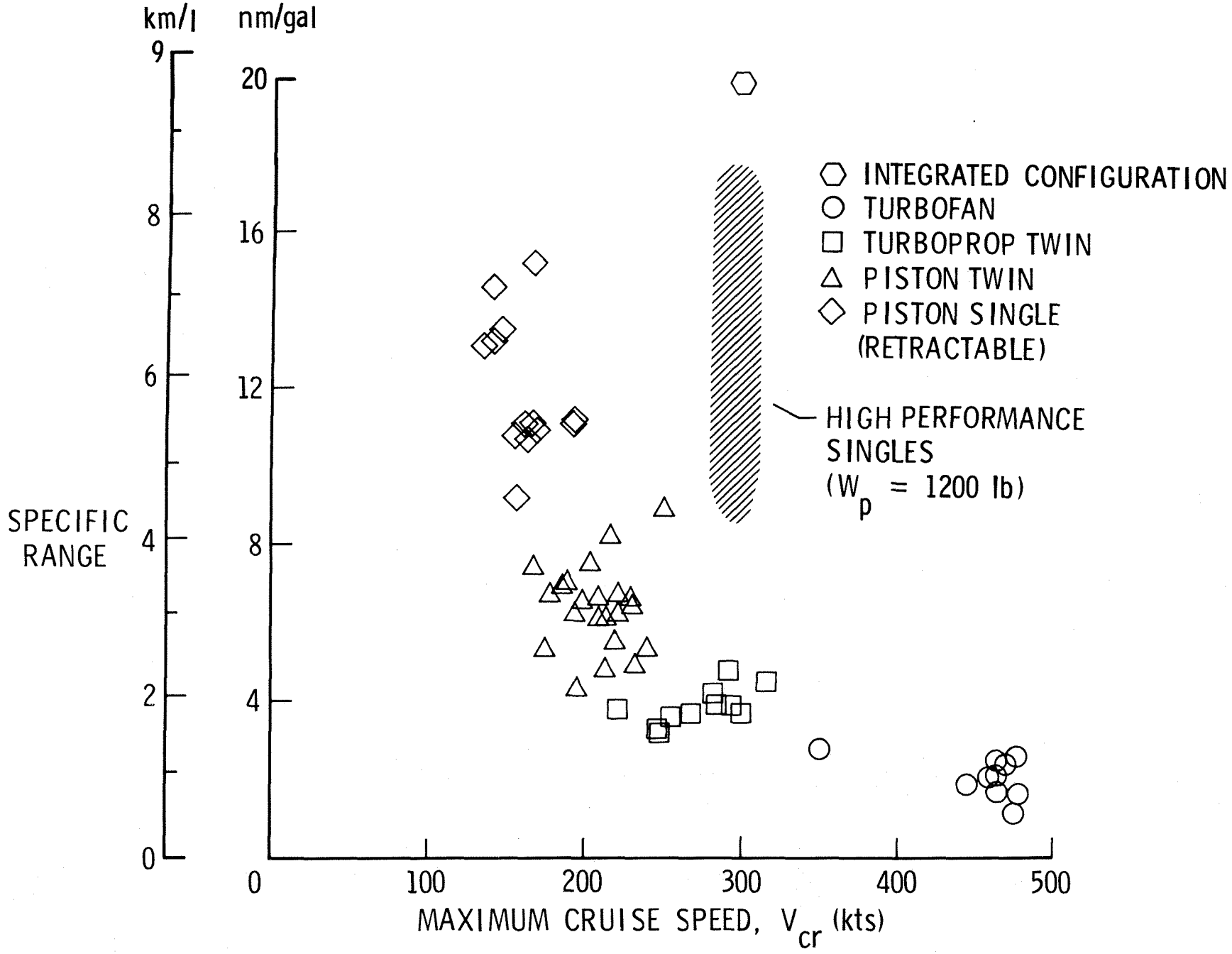

Figure 16. Comparison of Specific Range and Cruise Speed for Current and Advanced Technology Airplanes